*Article*

# Nitrogen Dioxide Optical Sensor Based on Redox-Active Tetrazolium/Pluronic Nanoparticles Embedded in PDMS Membranes

Esteban Araya-Hermosilla [1,*], Rodrigo Araya-Hermosilla [2], Francesco Visentin [3], Francesco Picchioni [4], Andrea Pucci [5,*] and Virgilio Mattoli [1,*]

1 Center for Materials Interfaces @SSSA, Istituto Italiano di Tecnologia, Viale Rinaldo Piaggio 34, 56025 Pontedera, Italy
2 Programa Institucional de Fomento a la Investigación, Desarrollo e Innovación (PIDi), Universidad Tecnológica Metropolitana, Ignacio Valdivieso 2409, San Joaquín, Santiago 8940577, Chile; rodrigo.araya@utem.cl
3 Bioinspired Soft Robotics Laboratory, Istituto Italiano di Tecnologia Viale Rinaldo Piaggio 34, 56025 Pontedera, Italy; francesco.visentin@iit.it
4 Department of Chemical Engineering—Product Technology, University of Groningen, Nijenborgh 4, 9747 AG Groningen, The Netherlands; f.picchioni@rug.nl
5 Department of Chemistry and Industrial Chemistry, University of Pisa, Via Moruzzi 13, 56124 Pisa, Italy
* Correspondence: esteban.araya@iit.it (E.A.-H.); andrea.pucci@unipi.it (A.P.); virgilio.mattoli@iit.it (V.M.); Tel.: +39-050-2219-270 (A.P.)

**Abstract:** Anthropogenic toxic vapour and gases are a worldwide threat for human health and to the environment. Therefore, it is crucial to develop highly sensitive devices that guarantee their rapid detection. Here, we prepared redox-switchable colloids by the in-situ reduction of 2,3,5-triphenyl-2H-tetrazolium (TTC) into triphenyl formazan (TF) stabilised with Pluronic F127 in aqueous media. The colloids were readily embedded in polydimethylsiloxane (PDMS) to produce a selective colour-switchable membrane for nitrogen dioxide ($NO_2$) detection. We found that the TTC reduction resulted in the production of red-coloured colloids with zeta potential between $-1$ to 3 mV and hydrodynamic diameters between 114 to 305 nm as hydrophobic dispersion in aqueous media stabilised by Pluronic at different molar concentrations. Moreover, the embedded colloids rendered highly homogenous red colour gas-permeable PDMS elastomeric membrane. Once exposed to $NO_2$, the membrane began to bleach after 30 s due to the oxidation of the embedded TF and undergo a complete decolouration after 180 s. Such features allowed the membrane integration in a low-cost sensing device that showed a high sensitivity and low detection limit to $NO_2$.

**Keywords:** redox-active organic nanoparticles; pluronic F-127; sensing membranes; wearable optical device

## 1. Introduction

Toxic vapours and gases produced by human activities are a worldwide threat for human and environmental health [1,2]. Nitrogen dioxide ($NO_2$) is a hazardous pollutant found mainly in industrialised and urbanised areas due to the oxidation of nitric oxide in the atmosphere [3]. It is a polar and acid oxide molecule that reacting with airborne water produces nitric acid, one of the components of acid rain [4]. At the industrial level, $NO_2$ is used as an intermediate in the production of nitric acid [5]. Regrettably, $NO_2$ is a corrosive gas that can causes severe damage to the skin, eyes, and respiratory tract [6,7], and can also be a factor of lung cancer [8]. Hence, it is important to develop cost-effective and highly sensitive wearable sensor devices that can sense $NO_2$ at low concentrations.

Metal oxide semiconductors (MOS) have dominated the field of sensors focused on detection of $NO_2$. Despite their high sensitivity and fast response [9], they require very

high working temperatures, which can possibly influence sensor morphology, excluding their utilisation for detecting flammable and explosive gases [10]. Therefore, low operating temperatures are preferred. For instance, Haidry et al. [11] fabricated a Pt/Cr-TiO$_2$/Pt-type sensor that reduced the operating temperature of the system from 400 to 200 °C, extending the lower limit of detection to concentrations of NO$_2$ below 10 ppm.

Flexible, light, stretchable, and wearable sensors could be powerful tools for detecting harmful gases, due to their ease of integration [12]. The fabrication of flexible sensors to detect NO$_2$ has been reported in the literature based on polymeric matrix doped with a conductive or semiconductive (nano)material. For instance, Khalifa et al. [13] designed a highly flexible wearable NO$_2$ sensor based on poly(vinylidene fluoride) (PVDF)/polyaniline (PANi)/graphitic-carbon nitride nanocomposite. Chen et al. [14] fabricate a wireless wearable NO$_2$ sensor by synthesising a nanocomposite constituted by ZnS nanoparticles distributed onto nitrogen-doped graphene, which was then deposited onto poly(ethylene terephthalate).

Although these systems showed good results in terms of response concentration, response and recovery time [15–19], and improvement in terms of temperature operation for MOS, chemoresistive sensors display certain drawbacks. The synthesis of the materials can be expensive and the process cumbersome [20,21]. Moreover, their sensing behaviour might be strongly dependent on ambient conditions such as temperature and humidity [22,23].

An effective alternative to chemoresistive sensors is represented by colorimetric sensors. For instance, Paliwal A. et al. [24] developed a surface plasmon resonance system by depositing a tungsten trioxide film on gold coated BK-7 glass prisms. The system was able to detect NO$_2$ at low concentrations (0.5 to 50 ppm), and showed a rapid optical response and recovery time (2 s for both parameters). Qin X. et al. [25] produced a simple material by immersing a silicon paper in a solution of N,N-dimethyl-p-phenylenediamine sulphate (DPD), which was integrated in a sensor chip. When DPD came into contact with NO$_2$, an azo compound was produced, and the sensor changed colour from light yellow to pink. The sensor showed a good detection limit of 10 ppb, but a sampling time of 5 min. Kang K. et al. [26] created a colorimetric film by spray coating a solution of N,N,N′,N′-tetramethyl-p-phenylenediamine (TMPD) on micro/nano wires of ZnO, synthetised on the surface of PDMS with micro-pillar arrays. TMPD provided the chromogenic response due to an oxidation reaction with NO$_2$ and the presence of the ZnO micro/nano wires increased the sensing performance by enhancing the sensing area. The sensor was able to detect NO$_2$ gas at concentrations down to 1–20 ppm, but the response time was very long due to the limited diffusion of the gas within the TMPD particles. Therefore, there is still room for the optimisation of NO$_2$ sensing in terms of fabrications routes, advanced soft materials and high-surface-area sensing probes.

In this respect, 2,3,5-triphenyl-2H-tetrazolium (TTC) is a promising redox-switchable molecule for the detection of toxic oxidant gases. TTC is a colourless compound composed of four aromatic rings and is soluble in aqueous media due to the positive charge on its tetrazolium rings (Figure 1). When TTC experiences reduction, it transforms into the hydrophobic red-coloured 1,3,5-triphenyl formazan (TF) [27] (Figure 1). Such chromogenic features make the switchable TTC/TF an ideal candidate for the detection of bacteria [28], the quantification of reducing carbonyl groups in cellulose [29], the determination of mammalian cell growth [30] and the sensing of metal ions [31]. Colloidal TTC/TF systems stabilised by polyelectrolytes or polymeric surfactants bearing aromatic groups have been previously reported in the literature to effectively detect NO$_2$ [27,32].

In the present work, the same sensing scheme is proposed and further optimised in terms of a more accurate sensing setup. Notably, the use of a polymeric surfactant without aromatic moieties demonstrates the efficiency of the hydrophobic interaction in the stabilisation of the colloidal sensing particles. In addition, the derived colloids are eventually incorporated for the first time in an elastomeric membrane, thus showing good sensitivity and fast detection to NO$_2$ gas at room temperature.
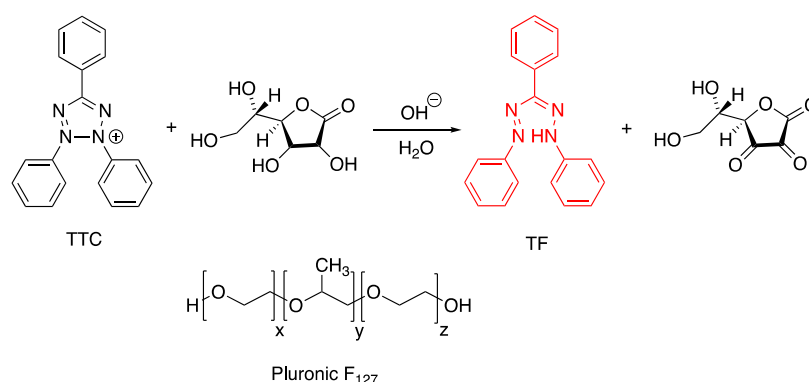
**Figure 1.** Chemical structures of 2,3,5-triphenyl-2H-tetrazolium (TTC), triphenyl formazan (TF) and Pluronic F127.

## 2. Material and Methods

### 2.1. Materials

2,3,5-triphenyl-2*H*-tetrazolium chloride (TTC) (Sigma-Aldrich, Milan, Italy, 98%), Pluronic F-127 (Sigma-Aldrich, MW 12600, Milano, Italy), ascorbic acid (Sigma-Aldrich, Milano, Italy), NaOH (Sigma-Aldrich), and Polydimethylsiloxane (PDMS) Sylgard 184 silicone elastomer base and curing agent (Dow Corning Corp, Midland, MI, USA) were used as received. Milli-Q water was used to prepare the different solutions. Calibrated mixture of $NO_2$ in nitrogen, 95.6 ppm mol, 5 L cylinder, 150 PSI (Nippon Gases Industrial S.r.l., Sesto Fiorentino (FI), Italy) was used in combination with a pressure reducer mod. RSD1SX 315/6 N2 MIX (Nippon Gases Industrial S.r.l., Sesto Fiorentino (FI), Italy).

### 2.2. Colour-Switchable Nanoparticle (CSN) Preparation

Stock aqueous solutions containing pluronic F127 at a concentration of 5 mM, ASC 0.1 M, TTC 0.1 M, and NaOH 1 M were prepared. Then, 1.5 mL of TTC and ASC were mixed with different amounts of Pluronic F127 stock solution to reach the desired polymer molar concentration from $5 \times 10^{-5}$ to $10^{-3}$ M, according to Tables S1–S5. Subsequently, 300 μL of NaOH (1 M) was added to start the reduction reaction. All the samples were prepared at a final volume of 15 mL.

### 2.3. CSN Characterisation

The hydrodynamic diameter and zeta potential of the resulting CSN were analysed by DLS at 25 °C using a Nano ZS zetasizer equipment (zetasizer Nano-ZS (Malvern Instruments, Malvern, UK)) with backscatter detection (173°), controlled by the Dispersion Technology Software (DTS 6.2, Malvern, UK). The results were considered valid under the criteria of the DTS 6.2 software (Malvern, UK).

SEM morphological characterisation of the CSN was performed by scanning electron microscopy (SEM, Dual Beam FIB/SEM Helios Nano-Lab 600i, FEI, Hillsboro, OR, USA), with a 10 KeV accelerating voltage and variable magnification. For SEM analysis, the samples were deposited on a copper grid and were left to dry at room temperature and ambient pressure without metallic coating, as reported in a previous work [33].

Differential scanning calorimetry (DSC) analysis was performed on selected colloidal suspensions after drying. The DSC experiments were conducted using a TA DSC250 under $N_2$ atmosphere (DSC, TA Instruments, New Castle, DE, USA). Samples were placed in aluminium pans and heated from 20 °C to 140 °C, cooled down to 20 °C, and then heated again to 140 °C at a scanning rate of 10 °C/min.

### 2.4. Membrane Preparation

A 1.5 mL volume of a solution containing 4.6 mg of CSN, which was prepared through the reduction of TTC (0.01 M) with ASC (0.01 M) in the presence of Pluronic at a concentration of $10^{-4}$ M, was mixed with 5 g of PDMS and 1 g of curing agent. The mixture was

then dried under low pressure by the help of a mechanical pump for 48 h. Then, the dried mixture was stirred manually until a homogenous red-coloured solution was obtained. The viscous red mixture was then degassed until no bubbles were seen using a mechanical pump. Afterward, the mixture composed of PDMS-CSN was spin-coated onto Teflon petri dishes for 60 s at a speed of 150 rpm and then placed in an oven at 120 °C overnight for curing, resulting in an elastomeric membrane being obtained. The obtained membranes had an average thickness of $1.07 \pm 0.05$ mm.

### 2.5. Detection of $NO_2$ Gas

The produced membrane was characterised to verify the colour-change behaviour in the presence of gaseous $NO_2$ produced by reacting metal copper with nitric acid, as follows.

$$Cu + HNO_3 \rightarrow Cu(NO_3)_2 + 2NO_2 \tag{1}$$

A preliminary visual evaluation was performed by directly exposing a piece of membrane to in-situ-generated $NO_2$ (200 mg metal copper with 18 mL of nitric acid). UV-VIS absorption spectra of the membrane sample were recorded before and after the exposition to the gas, by means of a LAMBDA 650 (PerkinElmer, Milano, Italy).

In a first test, to verify the overall device functionality, the device was connected with a 3-way round bottom flask (50 mL of volume), in which was produced an excess of $NO_2$, by putting 18 mL of nitric acid on 201 mg of metal copper. To preliminarily evaluate the sensitivity and detection limit of the membrane, an additional experiment was conducted by producing the $NO_2$ stoichiometrically, i.e., by adding single acid drop at time, for the first 3 measurements (lasting about 1000 s), and then adding two drops at time. Notably, in this case the membrane was connected with a 3-way round bottom flask (50 mL of volume), and connected with a small membrane pump (series D250, RS Pro, Sesto San Giovanni (MI), Italy) to generate a constant atmosphere flow (10 mL/s, measured) through the flask onto the sensing system. The transmittance variation of the membrane after the first drop of acid has been used for evaluating purpose (each drop of acid produces $2.46 \times 10^{-4}$ mol of $NO_2$, as by stoichiometry calculations, considering $HNO_3$ drops with a mass of $47.6 \pm 0.1$ mg).

Finally, a test with calibrated $NO_2$ in nitrogen gas mixture (95.6 ppm mol as measured by supplier) was performed in order to more consistently evaluate sensitivity and detection limit in term of volumetric concentration. The 5 L cylinder gas mixture was connected through a suitable pressure reducer and a three-way valve to the device; the three-way valve was also connected to a small-membrane pump (series D250, RS Pro), making it possible to select as input for the device either the $NO_2$ in nitrogen mixture or simply air provided by the pump. The air flow produced by the pump was about 10 mL/s (measured), while the gas mixture flow was regulated to a similar value by adjusting the output pressure of the regulator. The experiment was performed by alternating 210 s of air flow and 600 s of $NO_2$ mixture flow two times. The experiment was carried out on a freshly prepared membrane, after 120 min pre-conditioning exposure of the device to the $NO_2$ mixture flow (10 mL/s nominal), to avoid the edge of the measurement range.

### 2.6. Interference Gases

The sensing membranes were also tested in the presence of several interferences gases such as volatile organic compounds (VOC), such as chloroform ($CHCl_3$), tetrahydrofuran (THF), $CO_2$, $N_2O$, $H_2S$ and $NH_3$, during 4 min under saturation conditions. A saturated atmosphere of $CO_2$ was generated by dropping a solution of HCl (37%) to $CaCO_3$.

### 2.7. Optical Device Fabrication

As a low-cost alternative to spectrophotometric measurement, we developed LED/photodiode-based optical devices that can detect the change in the measured light intensity because of the decolouration of the redox-active membrane. The device hosts two membrane pieces that were cut using a razor blade with a final rectangular shape of $10 \times 12$ mm$^2$: the first one is colourless, being fully reduced by means of an excess of $NO_2$,

and acts as optical reference; the second pristine one acts as the optical sensing element. Notably, the sensor is based on a single green surface-mounted LED (LV CK7P, 505 nm peak wavelength, OSRAM, Munich, Germany) and two independent photoreceivers (photodiode TEMD5510FX01, Vishay SemiconductorsSelb, Germany), which are used to measure the relative change in the light intensity passing through two slices of the redox-active membrane. The LED generates a constant, unstructured source of light which is collimated to a constant light beam using an uncoated plano-convex lens (LA1540–N-BK7, Thorlabs, Newton, NJ, USA). The resultant beam of light is then split into two equal beams having 50% of the intensity by a beam splitter (BSW04, Thorlabs, Newton, NJ, USA), which is placed at 15 mm from the lens. The reflected beam is directed to a first photoreceiver placed behind one slice of the membrane, the reference one, acting as light waveguide. The transmitted beam, instead, is first reflected by an aluminium mirror (PF05-03-G01, Thorlabs, Newton, NJ, USA) and transmitted to a second photoresistor, also placed behind the other slice of the membrane, the sensing one, also acting as light waveguide. The overall holder enclosure is prepared by an additive manufacturing process. The photodiodes were electronically conditioned by direct connection with a low-cost system on the chip development board (CY8CKIT-059 PSOC, by Cypress, San Jose, CA, USA) without requiring any additional component. The system on the chip included, by firmware configuration, a transimpedance amplifier with software-selectable gain resistors and a 16-bit delta-sigma analogue-to-digital converter (ADC, resolution of <20 μV, sampling rate of 40 kSPS) used to amplify and acquire the signal directly form the photodiodes. The LED is also directly driven by the system on the chip board trough a dedicated current digital-to-analogue converter (DAC) set at 2 mA during measurements. Acquired signals were transmitted via USB to a PC for further absorbance/transmittance calculation, visualisation and recoding by ad-hoc-developed software. To measure the effect of the exposure to $NO_2$ vapours, only the freshly cut one of the two membranes is exposed to the environment, while the other one, already reduced with an excess of $NO_2$, is kept sealed. Figure 2 shows the schematic representation of the device. By computing the relative difference in the measured light intensity, it is possible to measure the amount of $NO_2$ vapour in the environment. Other details on the sensing device can be found in the Supplementary Materials. All the material (including hardware, firmware, and software) is available as an open-source resource at https://doi.org/10.5281/zenodo.5825639 (accessed on 1 June 2022).
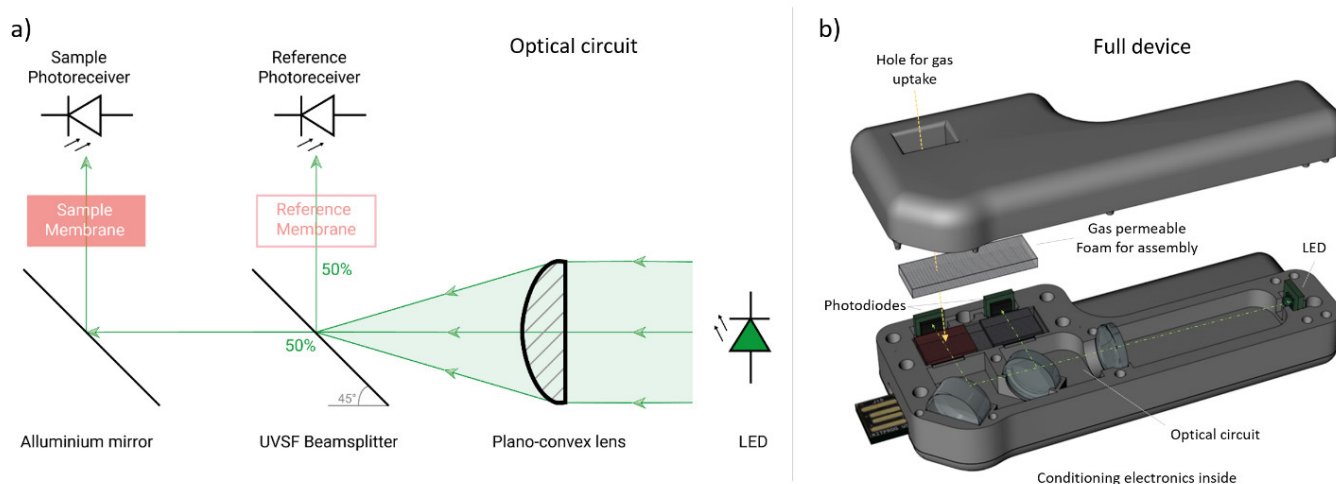


**Figure 2.** (**a**) Schematics of the optical circuit of the sensor device. A constant, unstructured source of light is generated by a LED connected to the control board. The light is then collimated to an UVSF beam splitter using a plano-convex lens. Half of the light intensity is then reflected towards the reference sample, while the remaining is transited towards the sensing (exposed) sample. (**b**) Semi-exploded view of the full device with optical circuit in view. Full details on device design can be found in Supplementary Materials (Figures S2–S5).

## 3. Results and Discussion

### 3.1. Synthesis of Colour-Switchable Nanoparticles (CSN)

Direct reduction of TTC to TF with ascorbic acid at basic pH (Figure 1) yields a red-coloured precipitate (Figure 3a(i)). Conversely, adding a certain amount of Pluronic F-127 to the reaction, a turbid red-coloured colloidal suspension is obtained. Different concentrations of Pluronic surfactant were tested, ranging from $10^{-5}$ to $10^{-3}$ M (Table S1 summarises the experimental conditions for all the tested colloids synthesis), and the investigated regime was effective at stabilising the colloidal dispersions (Figure 3a(ii–xii)).
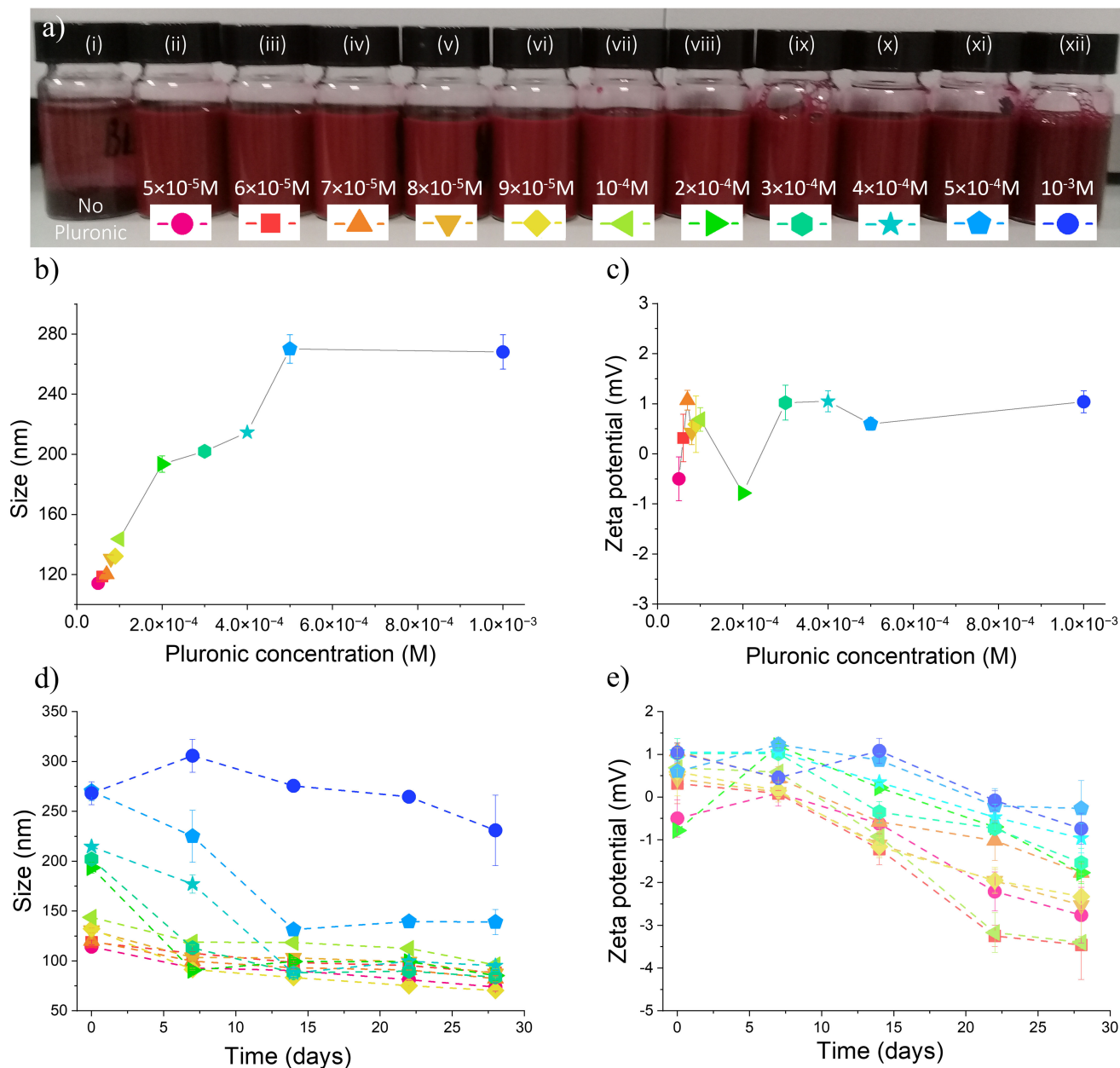


**Figure 3.** (**a**) Picture of TF particle samples produced by TTC reduction with ASC, in absence (**i**) and in presence of Pluronic surfactant stabiliser at different concentrations (**ii–xii**) (Pluronic concentrations reported in figure). Size (**b**) and zeta potential (**c**) of TF colloids stabilised with Pluronic. Colloid stability measured during 28 days: apparent size (**d**) and zeta potential (**e**) for different Pluronic concentrations (concentration following legend in (**a**)).

The mechanism of colloid formation can be explained in two steps. Firstly, the polymers form ion pair complexes with TTC by electrostatic interaction between their negatively charged aromatic group and the positively charged tetrazolium of TTC, and the derived complexes are stabilised by aromatic–aromatic interactions [34,35]. Secondly, owing to TF's hydrophobicity and electroneutrality, the colloids are considered to be precipitates of TF (hydrophobic core) stabilised by the polymers (hydrophilic shell) [27]. Considering that we used a nonionic polymeric surfactant as stabiliser, the hydrophobic interaction between the hydrophobic TF and the hydrophobic propylene oxide block of Pluronic possibly drives the co-assembly of the components in the form of colloids with an opalescent appearance [32,36].

The obtained CSN colloids were characterised by DLS and SEM imaging. The size and zeta potential of the different colloids are reported in the graphs in Figure 3 (see also Tables S1–S5). Colloidal particles display submicron sizes with diameters ranging from 114 to 305 nm (Figure 3b) with relatively good dispersion, showing polydispersity index (PDI) values from 0.23 to 0.35 [37] and zeta potential $\zeta$ close to zero (Figure 3c). By looking at the data, the polymer concentration clearly affects the colloid formation. The colloid size increases gradually with Pluronic concentration, reaching its maximum at $5 \times 10^{-4}$ M, which corresponds to the Pluronic critical micelle concentration (CMC) of $5.6 \times 10^{-4}$ M in aqueous media at room temperature [38]. This fact suggests that the surfactant polymer is mainly absorbed on the TF surface below the CMC, which is a phenomenon also reported in literature for other systems [36].

The colloids were stable for 28 days, but with a trend of decreasing size and a slight shift in zeta potential toward negative values (Figure 3d,e). Due to the nonionic nature of Pluronic and the low zeta potential value (that usually leads to aggregation), the great stability of the colloids could be explained by the steric hindrance of the polymer (thermodynamic stabilisation).

The morphology of dehydrated TF nanoparticles was verified by SEM analysis. SEM micrographs of the nanoparticles stabilised with Pluronic at selected concentrations ($5 \times 10^{-5}$ M, $1 \times 10^{-4}$ M, and $1 \times 10^{-3}$ M) and of the precipitate obtained in the absence of it are reported in Figure 4 for comparison. The particles showed a much smaller size compared to the size evaluated by DLS, for the concentrations below CMC ($5 \times 10^{-5}$ M and $10^{-4}$ M). This suggests that, for these surfactant concentrations, the colloids are formed by core–shell-like particles, where the hydrophobic TF core is surrounded by a co-assembled and highly hydrated Pluronic shell. On the other hand, in the presence of Pluronic at a concentration of $10^{-3}$ M, the size is comparable to that of the one measured by DLS, which is in agreement with the considerations reported earlier.

Since the process for fabricating the sensing membrane (see next section) involves relatively high heating during the PDMS curing process, we evaluated the thermal stability of nanoparticles by DSC analysis, performing the measurements on TTC, on Pluronic as is, and on the dried colloids composed of TF (0.01 M) and Pluronic at the same selected concentrations ($5 \times 10^{-5}$ M, $10^{-4}$ M, and $10^{-3}$ M) (see Figure S1). The DSC curve of pure Pluronic showed a sharp endothermal peak at 57 °C, corresponding to its melting point [39]. Conversely, TTC did not shown any thermal transition, thus indicating its stability in the temperature range of interest (20–140 °C). As expected, the colloids showed only the endothermal peak attributed to the Pluronic melting point, whose amplitude (integral of the peak) is in agreement with its concentration.

### 3.2. Production of Colour-Changing Membranes and NO$_2$ Detection

To fabricate the coloured sensing membranes, colloids containing 0.1 M of TF and a Pluronic concentration of $10^{-4}$ M were selected, since they showed suitable colloidal size in the submicron region, stability, and the amount of Pluronic did not affect the crosslinking of the PDMS matrix. PDMS was cured at 120 °C overnight, thus providing a homogenous transparent red-coloured membrane (see Figure 5, and Section 2.3 for fabrication details).

Because PDMS is highly permeable to gases, the membrane was then utilised for the optical detection of high-oxidant gases such as $NO_2$.
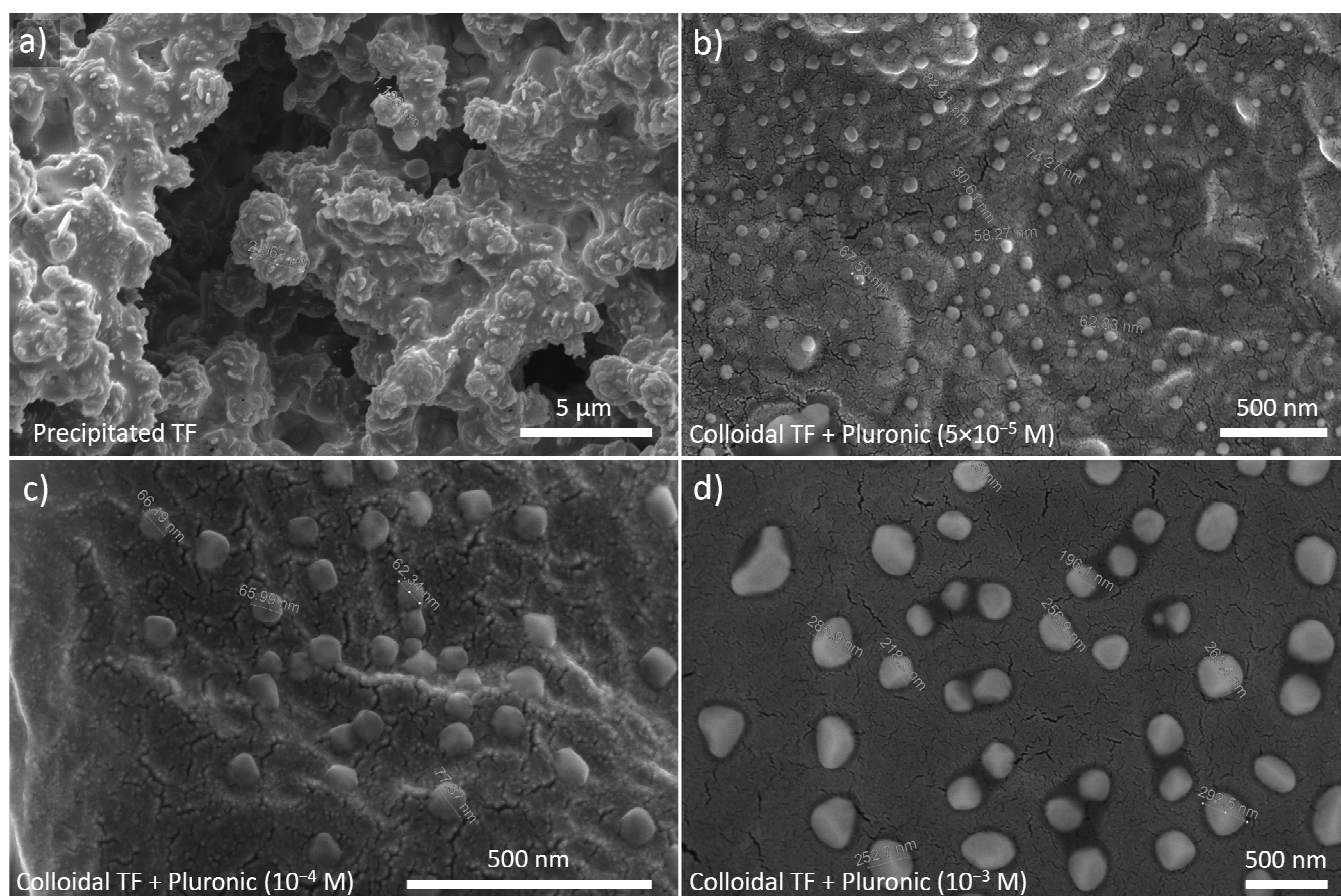


**Figure 4.** SEM pictures of TF precipitates after reduction of $10^{-2}$ M of TTC with ASC (**a**) and of dehydrated TF colloidal particle samples, stabilised with Pluronic at different concentrations: $5 \times 10^{-5}$ M (**b**), $10^{-4}$ M (**c**) and $10^{-3}$ M (**d**).

Notably, when exposed directly to $NO_2$, the membrane quickly decoloured, becoming completely transparent (see Figure 5a). The UV-Vis spectra show a broad absorbance peak around 490 nm for the pristine membrane, which is responsible for the red colouration and typical of the TF dye. After exposure to $NO_2$, the TF nanoparticles dispersed in the PDMS matrix oxidised back to the colourless form TTC, and the membrane absorption spectra become flat (see Figure 5b). Thanks to this chromogenic response, the membrane can therefore act as a chemo-colorimetric sensor working in the 480–510 nm spectral range. To exploit such colorimetric gas sensing features, we integrated the membrane in a low-cost sensing device, used as proof of concept. The idea is to use a double beam system, in which one membrane, the coloured one, acts as a sensor that is put in contact with the gas, while the other one, fully reduced, is used as a reference. Due to their thickness (about 1 mm), the membranes can be used as an optical waveguide, having a sufficiently long optical path (on the order of 1 cm) for the optical measurements. The system is based on a single LED emitter with a relatively narrow peak emission at 505 nm (in the range of interest), and two visible photodiodes that collect the light passing along the two membranes (cut to have an optical path of 1 cm). The current signal from the photodiodes (proportional to incoming light) is converted into voltage by a transimpedance amplifier, and then digitalised. Technical details related to the implementation of the device are reported in the Materials and Methods section and in the Supporting Information (Figures S2–S5). As an indicator of $NO_2$ detection, we evaluated the variation of the normalised transmittance $T_n$

(normalised with respect to the final transmittance value of the sensing membrane once fully reduced), calculated from the acquired voltage signals as follows:

$$T_n = \frac{V_{Sens}}{V_{Ref}} \cdot \frac{V^0_{Ref}}{V^0_{Sens}} \tag{2}$$

where $V_{Sens}$ and $V_{Ref}$ are the signals for the sensing and reference membranes, respectively, and $V^0{}_{Sens}$ and $V^0{}_{Ref}$ are the same at saturation (i.e., sensing membrane completely oxidised and decoloured).
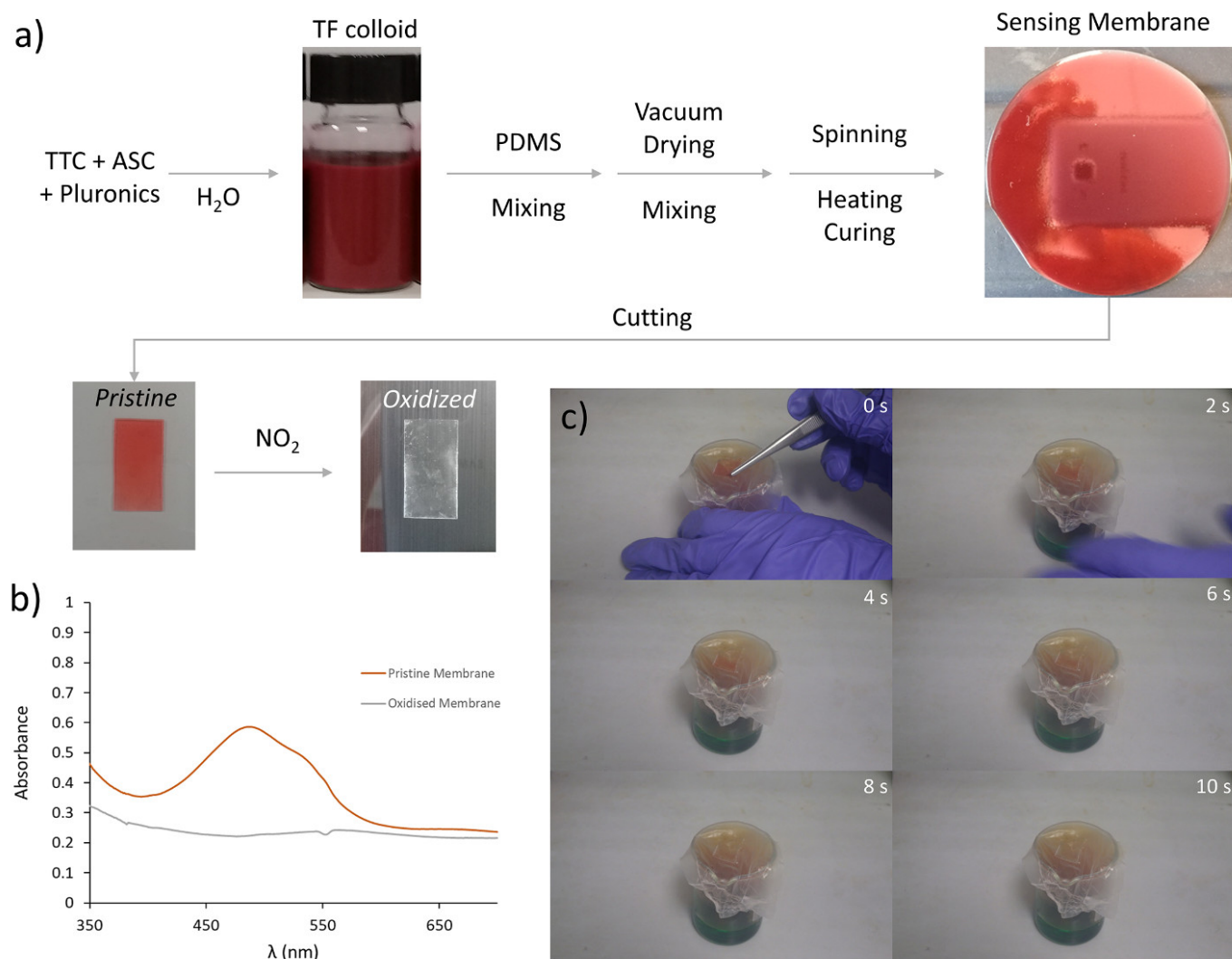


**Figure 5.** (**a**) Sensing membrane fabrication scheme. (**b**) UV-Vis absorbance spectra of the membrane as prepared (orange) and after full oxidation by NO$_2$ exposure (grey). (**c**) Demonstration of rapid oxidation of the coloured sensing membrane with an excess of nitrous gas.

As a first attempt, to evaluate the kinetics of the process, we exposed the fresh sensing membrane to a high concentration of NO$_2$ gas (2.6 M) through the dedicated opening in the device. The red-coloured membrane began to bleach after 30 s of NO$_2$ evolution and reached full discolouration after 180 s, as indicated by the transmittance values (See Figure S6).

The selectivity of membrane discolouration was tested by exposing it to different interference gases, such as CHCl$_3$, THF, CO$_2$, N$_2$O, H$_2$S and NH$_3$, under saturated conditions. Remarkably, the membrane did not show any significant variation in its optical features

even after 4 min of gas exposure, as shown by the UV-Vis spectra and optical pictures acquired before and after exposure to gas (see Figure 6).
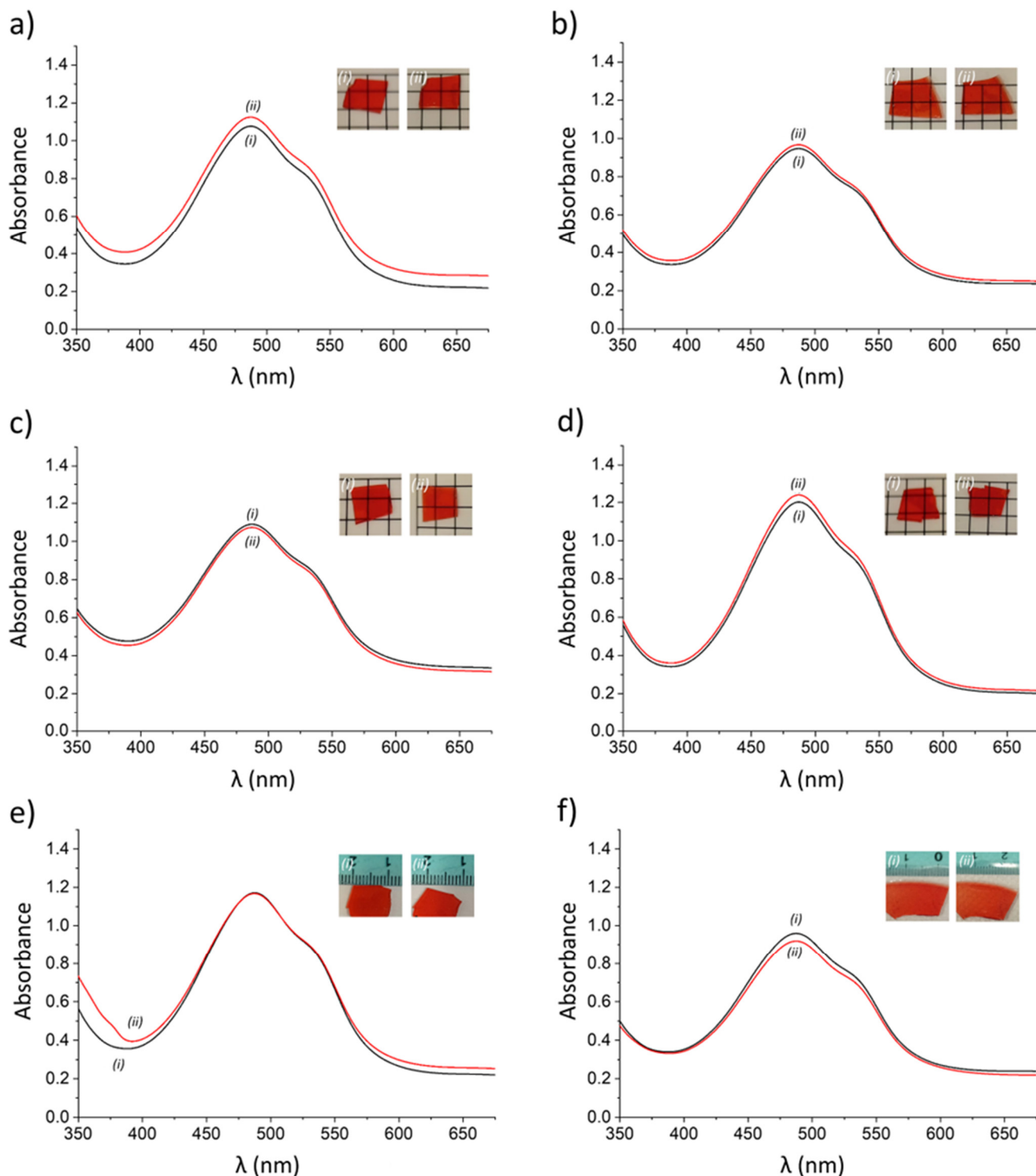


**Figure 6.** UV-Vis absorption spectra and photos of the membrane before (**i**) and after (**ii**) exposure to a saturated atmosphere of (**a**) chloroform, (**b**) tetrahydrofuran, (**c**) $CO_2$, (**d**) $NH_3$, (**e**) $N_2O$, and (**f**) $H_2S$ for 4 min.

Since the membrane showed high selectivity towards $NO_2$ gas, the sensing system was studied systematically to evaluate the sensitivity and the detection limit. More precisely, the experiments were repeated in a more controlled way, i.e., by slowly dropping nitric

acid solution onto metallic copper to produce a precise amount of $NO_2$ within a 50 mL three-way flask, and pumping at 10 mL/s towards the sensor device (Figure 7b). The signals were recorded continuously, and the acid dropping made it possible to continue until the signal reached a plateau. The measurement was stopped at complete oxidation of the membrane, and the normalised transmittance finally calculated (Figure 7c,d).
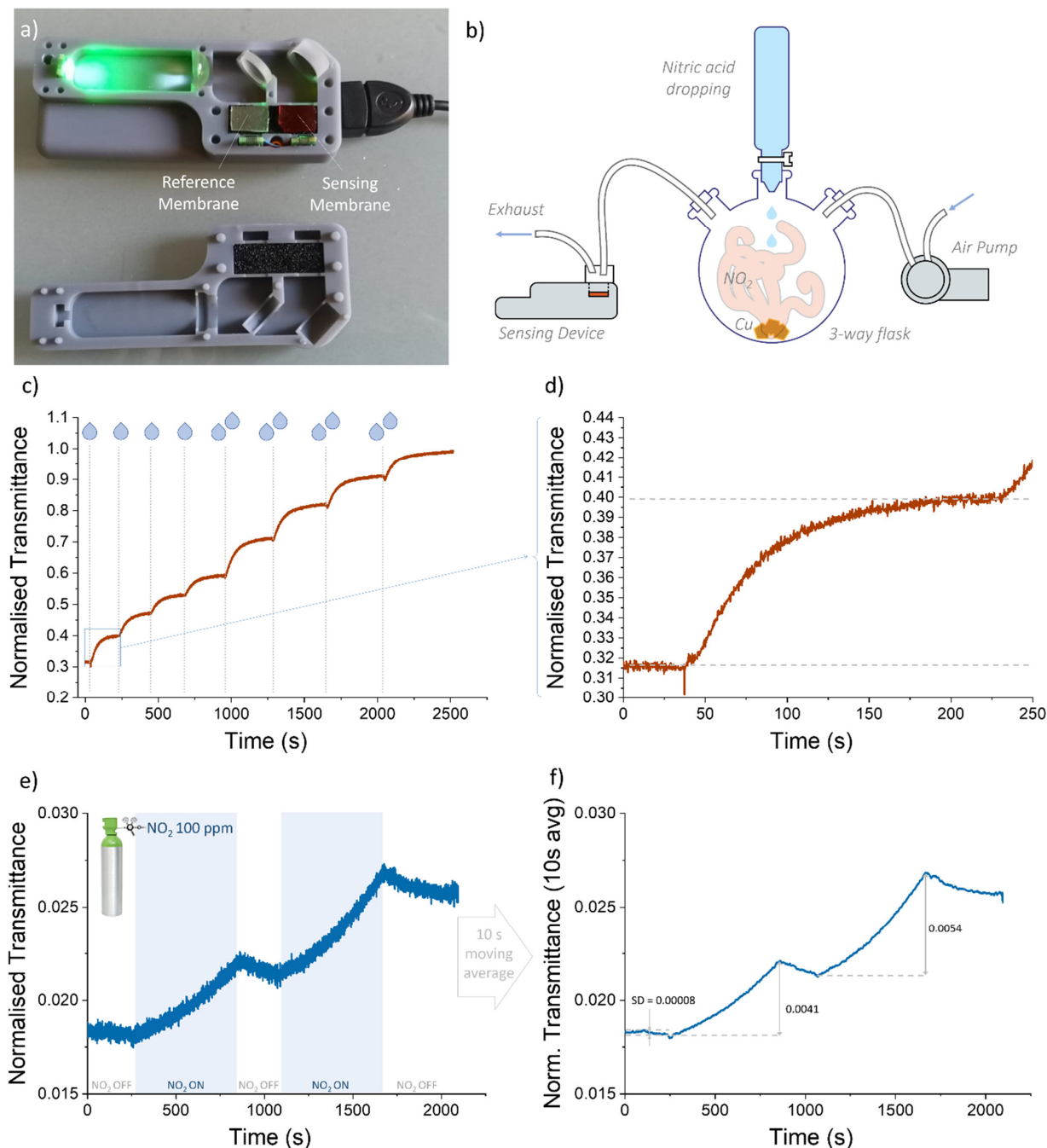


**Figure 7.** Membrane $NO_2$ sensitive experiment. (**a**) Picture of the colorimetric device. (**b**) Scheme of the experimental setup. (**c**) Transmittance variation during time when the membrane is exposed to $NO_2$ gas (the addition of a single drop or double drops is evidenced). (**d**) Transmittance variation of the membrane when is exposed to a first single drop (each drop corresponds to the development of $2.46 \times 10^{-4}$ mol of $NO_2$). (**e**) Transmittance variation of the membrane (fresh one) when exposed to a controlled flow of constant 100 ppm calibrated concentration of $NO_2$ in nitrogen. (**f**) The same data after applying 10 s moving average filter.

The sensitivity and the detection limit for $NO_2$ measurement were evaluated on the first drop of nitric acid (each drop produce around $2.5 \times 10^{-4}$ mol of $NO_2$), where the sensor response is higher. The sensitivity can be roughly estimated by considering the kinetics of the reaction and the flow. For the first drop, air was flowed for 200 s (corresponding to 2000 mL) with an average $NO_2$ concentration of $1.25 \times 10^{-4}$ M (for a total flowing amount of $2.5 \times 10^{-4}$ mol); this led to a variation of 0.083 of $T_n$, which corresponded to a minimum sensitivity of 3.32 $M^{-1}$ $s^{-1}$ in terms of normalised transmittance vs. concentration, or 332 $mol^{-1}$ $NO_2$ if we consider the amounts. The detection limit, i.e., the minimum detectable amount of gas, can be more easily evaluated when considering the noise to be 3 times the standard deviation of the background, 0.0045 in terms of $T_n$, corresponding to $1.3 \times 10^{-5}$ mol.

Finally, to further assess the viability of the proposed sensing device, we also evaluated the response of the system to a pre-calibrated mixture of $NO_2$ in $N_2$ with a constant nominal concentration of 100 ppm (95.6 ppm mol, as measured by the supplier), for a more direct correlation of characteristics with volumetric concentration. The experiment was performed by alternating the flow of the constant-concentration $NO_2$ mixture with flow of simple air, as reported in Figure 7e. The response of the system to the 100 ppm $NO_2$ mixture is rather clear, even if a small relaxation effect is evidenced after the interruption of the $NO_2$ flow. This is possibly due to the rearrangement toward equilibrium of oxidation front thought the thickness of the membrane. Since temporal constraints are not stringent, the obtained data (acquired at four samples per second) can be further filtered with a moving average filter, as reported in Figure 7f, in which a 10 s window was chosen. From the filtered data, the sensitivity of the system can be evaluated in terms of volumetric concentration. In particular, given a $T_n$ increase of $0.0047 \pm 0.0006$ for a 600 s exposure at 100 ppm of $NO_2$, it is possible to calculate a sensitivity of $8 \pm 1 \times 10^{-6}$ $ppm^{-1}$ $s^{-1}$. The detection limit can also be evaluated in this case, considered as 3 times the standard deviation of the background (0.00008 in terms of $T_n$, calculated using a background sampling of 800 s, filtered as above), resulting in a value of 5 ppm for a sampling time of 10 min.

Overall, the results obtained in this work are consistent in terms of the combination of detection limit (5 ppm), sensitivity ($8 \pm 1 \times 10^{-6}$ $ppm^{-1}$ $s^{-1}$) and fast response when compared with those presented in the recent literature (see Introduction). For instance, a surface plasmon resonance system based on $WO_3$ thin films was able to detect $NO_2$ in a range of 0.5–10 ppm at room temperature [24]. Moreover, ZnO nanostructures decorated with Au showed a sensing (optical) response to $NO_2$ gases in a range of 5–10 ppm and at temperatures between 150 and 300 °C [40–42].

## 4. Conclusions

In conclusion, we reported the design and the preparation of a new PDMS sensing membrane able to detect $NO_2$ gas via an optical output. The sensing system was based on a redox-active organic colloid prepared via a simple, cheap, and green method, using as starting materials the redox-active TTC and the amphiphilic Pluronic F-127. The reduction of TTC with ASC at basic pH produced TF colloids stabilised by the amphiphilic polymer displaying hydrodynamic diameters ranging from 114 to 305 nm, reasonably low size polydispersity, and zeta potential close to zero mV. The colloids demonstrated stability for 28 days with a tendency to decrease in size. The TF/Pluronic colloids were homogeneously dispersed in the PDMS matrix, which was then cured at 120 °C without affecting the stability of the chromogenic TF red dye. The derived, red-coloured membranes were eventually integrated into a low-cost device, which was able to selectively sense $NO_2$ gas due to the fast TF $\rightarrow$ TTC conversion, demonstrating a bleaching process in the range of seconds and with a sensitivity of $8 \times 10^{-6}$ $ppm^{-1}$ $s^{-1}$ $NO_2$, and a detection limit of 5 ppm for a 10 min sampling. These elastomeric membranes are envisioned to be used for the fabrication of chromogenic and light-flexible sensor devices for the detection of toxic oxidising agents and personal exposure assessment. In this sense, the easy fabrication in terms of colloids preparation, membrane and device fabrication allow tailoring the

sensing properties of the systems as desired, and further improvements could be designed to minimise the detection time and sensitivity.

## References

1. Tang, S.; Guo, L.; Zhu, S.; Ma, L.; Tian, Y. Paper-Like Visual Indicator Films for Harmful Hydrophilic Liquids and Vapors. *ACS Appl. Polym. Mater.* **2021**, *3*, 4027–4034. [CrossRef]
2. Barea, E.; Montoro, C.; Navarro, J.A.R. Toxic Gas Removal-Metal-Organic Frameworks for the Capture and Degradation of Toxic Gases and Vapours. *Chem. Soc. Rev.* **2014**, *43*, 5419–5430. [CrossRef]
3. Harrison, R.M.; Shi, J.P. Sources of Nitrogen Dioxide in Winter Smog Episodes. *Sci. Total Environ.* **1996**, *189–190*, 391–399. [CrossRef]
4. Breeze, P. Combustion Plant Emissions: Sulfur Dioxide, Nitrogen Oxides, and Acid Rain. In *Electricity Generation and the Environment*; ELSEVIER: Amsterdam, The Netherlands, 2017. [CrossRef]
5. Cheremisinoff, P.N. Industry Profile—Fertilizers. In *Waste Minimization and Cost Reduction for the Process Industries*; William Andrew Publishing: Norwich, NY, USA, 1995. [CrossRef]
6. Liu, S.K.; Cai, S.; Chen, Y.; Xiao, B.; Chen, P.; Xiang, X.D. The Effect of Pollutional Haze on Pulmonary Function. *J. Thorac. Dis.* **2016**, *8*, E41–E56. [CrossRef] [PubMed]
7. WHO. *WHO Air Quality Guidelines: Global Update 2005: Report on a Working Group Meeting, Bonn, Germany, 18–20 October 2005*; World Health Organization, Regional Office for Europe: Geneva, Switzerland, 2006.
8. Hamra, G.B.; Laden, F.; Cohen, A.J.; Raaschou-Nielsen, O.; Brauer, M.; Loomis, D. Lung Cancer and Exposure to Nitrogen Dioxide and Traffic: A Systematic Review and Meta-Analysis. *Environ. Health Perspect.* **2015**, *123*, 1107–1112. [CrossRef]
9. Kanaparthi, S.; Govind Singh, S. Highly Sensitive and Ultra-Fast Responsive Ammonia Gas Sensor Based on 2D ZnO Nanoflakes. *Mater. Sci. Energy Technol.* **2019**, *3*, 91–96. [CrossRef]
10. Xuan, J.; Zhao, G.; Sun, M.; Jia, F.; Wang, X.; Zhou, T.; Yin, G.; Liu, B. Low-Temperature Operating ZnO-Based $NO_2$ sensors: A Review. *RSC Adv.* **2020**, *10*, 39786–39807. [CrossRef] [PubMed]
11. Saruhan, B.; Lontio Fomekong, R.; Nahirniak, S. Review: Influences of Semiconductor Metal Oxide Properties on Gas Sensing Characteristics. *Front. Sens.* **2021**, *2*, 657931. [CrossRef]
12. Xu, M.; Obodo, D.; Yadavalli, V.K. The Design, Fabrication, and Applications of Flexible Biosensing Devices. *Biosens. Bioelectron.* **2019**, *124–125*, 96–114. [CrossRef]
13. Khalifa, M.; Anandhan, S. Highly Sensitive and Wearable $NO_2$ gas Sensor Based on PVDF Nanofabric Containing Embedded Polyaniline/g-$C_3N_4$ nanosheet Composites. *Nanotechnology* **2021**, *32*, 485504. [CrossRef] [PubMed]
14. Chen, X.; Wang, T.; Han, Y.; Lv, W.; Li, B.; Su, C.; Zeng, M.; Yang, J.; Hu, N.; Su, Y.; et al. Wearable $NO_2$ Sensing and Wireless Application Based on ZnS Nanoparticles/Nitrogen-Doped Reduced Graphene Oxide. *Sens. Actuators B Chem.* **2021**, *345*, 130423. [CrossRef]

15. Yu, L.; Guo, F.; Liu, S.; Yang, B.; Jiang, Y.; Qi, L.; Fan, X. Both Oxygen Vacancies Defects and Porosity Facilitated $NO_2$ Gas Sensing Response in 2D ZnO Nanowalls at Room Temperature. *J. Alloys Compd.* **2016**, *682*, 352–356. [CrossRef]

16. Chen, R.; Wang, J.; Xiang, L. Facile Synthesis of Mesoporous ZnO Sheets Assembled by Small Nanoparticles for Enhanced $NO_2$ Sensing Performance at Room Temperature. *Sens. Actuators B Chem.* **2018**, *270*, 207–215. [CrossRef]

17. Novikov, S.; Lebedeva, N.; Satrapinski, A.; Walden, J.; Davydov, V.; Lebedev, A. Graphene Based Sensor for Environmental Monitoring of $NO_2$. *Sens. Actuators B Chem.* **2016**, *236*, 1054–1060. [CrossRef]

18. Singh, A.K.; Uddin, M.A.; Tolson, J.T.; Maire-Afeli, H.; Sbrockey, N.; Tompa, G.S.; Spencer, M.G.; Vogt, T.; Sudarshan, T.S.; Koley, G. Electrically Tunable Molecular Doping of Graphene. *Appl. Phys. Lett.* **2013**, *102*, 043101. [CrossRef]

19. Chen, X.; Zhao, S.; Zhou, P.; Cui, B.; Liu, W.; Wei, D.; Shen, Y. Room-Temperature $NO_2$ Sensing Properties and Mechanism of CuO Nanorods with Au Functionalization. *Sens. Actuators B Chem.* **2020**, *328*, 129070. [CrossRef]

20. Kang, J.Y.; Koo, W.T.; Jang, J.S.; Kim, D.H.; Jeong, Y.J.; Kim, R.; Ahn, J.; Choi, S.J.; Kim, I.D. 2D Layer Assembly of Pt-ZnO Nanoparticles on Reduced Graphene Oxide for Flexible $NO_2$ Sensors. *Sens. Actuators B Chem.* **2020**, *331*, 129371. [CrossRef]

21. Fan, H.; Li, H.; Han, J.; McKeever, N.; Yu, J.; Katz, H.E. A Humid-Air-Operable, $NO_2$-Responsive Polymer Transistor Series Circuit with Improved Signal-to-Drift Ratio Based on Polymer Semiconductor Oxidation. *ACS Sens.* **2019**, *4*, 3240–3247. [CrossRef] [PubMed]

22. Choi, S.J.; Choi, H.J.; Koo, W.T.; Huh, D.; Lee, H.; Kim, I.D. Metal-Organic Framework-Templated PdO-$Co_3O_4$ Nanocubes Functionalized by SWCNTs: Improved $NO_2$ Reaction Kinetics on Flexible Heating Film. *ACS Appl. Mater. Interfaces* **2017**, *9*, 40593–40603. [CrossRef]

23. Kim, S.H.; Yang, H.; Yang, S.Y.; Hong, K.; Choi, D.; Yang, C.; Chung, D.S.; Park, C.E. Effect of Water in Ambient Air on Hysteresis in Pentacene Field-Effect Transistors Containing Gate Dielectrics Coated with Polymers with Different Functional Groups. *Org. Electron.* **2008**, *9*, 673–677. [CrossRef]

24. Paliwal, A.; Sharma, A.; Tomar, M.; Gupta, V. Room Temperature Detection of $NO_2$ Gas Using Optical Sensor Based on Surface Plasmon Resonance Technique. *Sens. Actuators B Chem.* **2015**, *216*, 497–503. [CrossRef]

25. Qin, X.; Yu, J.; Jiao, M.; Shan, X.; Xian, X.; Wang, D.; Tao, N. Integrating Electrochemical and Colorimetric Sensors with a Webcam Readout for Multiple Gas Detection. *Anal. Chem.* **2019**, *92*, 799–805. [CrossRef] [PubMed]

26. Kang, K.; Park, J.; Kim, B.; Na, K.; Cho, I.; Rho, J.; Yang, D.; Lee, J.Y.; Park, I. Self-Powered Gas Sensor Based on a Photovoltaic Cell and a Colorimetric Film with Hierarchical Micro/Nanostructures. *ACS Appl. Mater. Interfaces* **2020**, *12*, 39024–39032. [CrossRef] [PubMed]

27. Flores, M.E.; Garcés-Jerez, P.; Fernández, D.; Aros-Perez, G.; González-Cabrera, D.; Álvarez, E.; Cañas, I.; Oyarzun-Ampuero, F.; Moreno-Villoslada, I. Facile Formation of Redox-Active Totally Organic Nanoparticles in Water by In Situ Reduction of Organic Precursors Stabilized through Aromatic–Aromatic Interactions by Aromatic Polyelectrolytes. *Macromol. Rapid Commun.* **2016**, *37*, 1729–1734. [CrossRef] [PubMed]

28. Sabaeifard, P.; Abdi-Ali, A.; Soudi, M.R.; Dinarvand, R. Optimization of Tetrazolium Salt Assay for Pseudomonas Aeruginosa Biofilm Using Microtiter Plate Method. *J. Microbiol. Methods* **2014**, *105*, 134–140. [CrossRef]

29. Strlič, M.; Pihlar, B. Determination of Reducing Carbonyl Groups in Cellulose in the Solvent System LiCl/N,N-Dimethylacetamide. *Fresenius J. Anal. Chem.* **1997**, *357*, 670–675. [CrossRef]

30. Otero, A.J.; Rodríguez, I.; Falero, G. 2,3,5-Triphenyl Tetrazolium Chloride (TTC) Reduction as Exponential Growth Phase Marker for Mammalian Cells in Culture and for Myeloma Hybridization Experiments. *Cytotechnology* **1991**, *6*, 137–142. [CrossRef]

31. Nagaraja, P.; Hemantha Kumar, M.S.; Yathirajan, H.S. Silver-Enhanced Reduction of 2,3,5-Triphenyl-2H-Tetrazolium by Semicarbazide for the Spectrophotometric Determination of Traces of Silver(I). *Anal. Sci.* **2002**, *18*, 815–817. [CrossRef]

32. Araya-Hermosilla, E.; Catalán-Toledo, J.; Muñoz-Suescun, F.; Oyarzun-Ampuero, F.; Raffa, P.; Polgar, L.M.; Picchioni, F.; Moreno-Villoslada, I. Totally Organic Redox-Active PH-Sensitive Nanoparticles Stabilized by Amphiphilic Aromatic Polyketones. *J. Phys. Chem. B* **2018**, *122*, 1747–1755. [CrossRef]

33. Araya-Hermosilla, E.; Moreno-Villoslada, I.; Araya-Hermosilla, R.; Flores, M.E.; Raffa, P.; Biver, T.; Pucci, A.; Picchioni, F.; Mattoli, V. Ph-Responsive Polyketone/5,10,15,20-Tetrakis-(Sulfonatophenyl)Porphyrin Supramolecular Submicron Colloidal Structures. *Polymers* **2020**, *12*, 2017. [CrossRef]

34. Moreno-Villoslada, I.; Soto, M.; González, F.; Montero-Silva, F.; Hess, S.; Takemura, I.; Oyaizu, K.; Nishide, H. Reduction of 2,3,5-Triphenyl-2H-Tetrazolium Chloride in the Presence of Polyelectrolytes Containing 4-Styrenesulfonate Moieties. *J. Phys. Chem. B* **2008**, *112*, 5350–5354. [CrossRef]

35. Moreno-Villoslada, I.; Torres, C.; González, F.; Soto, M.; Nishide, H. Stacking of 2,3,5-Triphenyl-2H-Tetrazolium Chloride onto Polyelectrolytes Containing 4-Styrenesulfonate Groups. *J. Phys. Chem. B* **2008**, *112*, 11244–11249. [CrossRef]

36. Santander-Ortega, M.J.; Jódar-Reyes, A.B.; Csaba, N.; Bastos-González, D.; Ortega-Vinuesa, J.L. Colloidal Stability of Pluronic F68-Coated PLGA Nanoparticles: A Variety of Stabilisation Mechanisms. *J. Colloid Interface Sci.* **2006**, *302*, 522–529. [CrossRef]

37. Raval, N.; Maheshwari, R.; Kalyane, D.; Youngren-Ortiz, S.R.; Chougule, M.B.; Tekade, R.K. Importance of Physicochemical Characterization of Nanoparticles in Pharmaceutical Product Development. In *Basic Fundamentals of Drug Delivery*; ACADEMIC PRESS: Cambridge, MA, USA, 2018. [CrossRef]

38. Rahme, K.; Oberdisse, J.; Schweins, R.; Gaillard, C.; Marty, J.D.; Mingotaud, C.; Gauffre, F. Pluronics-Stabilized Gold Nanoparticles: Investigation of the Structure of the Polymer-Particle Hybrid. *ChemPhysChem* **2008**, *9*, 2230–2236. [CrossRef]

39. Karolewicz, B.; Gajda, M.; Pluta, J.; Górniak, A. Dissolution Study and Thermal Analysis of Fenofibrate–Pluronic F127 Solid Dispersions. *J. Therm. Anal. Calorim.* **2015**, *125*, 751–757. [CrossRef]

40. Chen, X.; Shen, Y.; Zhong, X.; Li, T.; Zhao, S.; Zhou, P.; Han, C.; Wei, D.; Shen, Y. Synthesis of ZnO Nanowires/Au Nanoparticles Hybrid by a Facile One-Pot Method and Their Enhanced $NO_2$ Sensing Properties. *J. Alloys Compd.* **2019**, *783*, 503–512. [CrossRef]

41. Ponnuvelu, D.V.; Dhakshinamoorthy, J.; Prasad, A.K.; Dhara, S.; Kamruddin, M.; Pullithadathil, B. Geometrically Controlled Au-Decorated ZnO Heterojunction Nanostructures for $NO_2$ Detection. *ACS Appl. Nano Mater.* **2020**, *3*, 5898–5909. [CrossRef]

42. Shingange, K.; Swart, H.C.; Mhlongo, G.H. Au Functionalized ZnO Rose-like Hierarchical Structures and Their Enhanced $NO_2$ Sensing Performance. *Phys. B Condens. Matter* **2018**, *535*, 216–220. [CrossRef]